IEEE Access
Multidisciplinary | Rapid Review | Open Access Journal

Received January 22, 2020, accepted February 4, 2020, date of publication February 10, 2020, date of current version February 17, 2020.

Digital Object Identifier 10.1109/ACCESS.2020.2972572

Soil Discharging Mechanism Utilizing Water Jetting to Improve Excavation Depth for Seabed Drilling Explorer

KEITA ISAKA[1], KAZUKI TSUMURA[1], TOMOKI WATANABE[1], WATARU TOYAMA[2], MANABU OKUI[2], HIROSHI YOSHIDA[3], AND TARO NAKAMURA[2], (Member, IEEE)

[1]Graduate School of Science and Engineering, Chuo University, Tokyo 112-8551, Japan
[2]Faculty of Science and Engineering, Chuo University, Tokyo 112-8551, Japan
[3]Marine Technology and Engineering Center, Japan Agency for Marine-Earth Science and Technology, Yokosuka 237-0061, Japan

Corresponding author: Keita Isaka (k_isaka@bio.mech.chuo-u.ac.jp)

ABSTRACT Seabed mineral resources have been found on the bottom of the ocean, and to utilize them, samples must be taken and analyzed. This study develops a seafloor robotic explorer that can excavate and sample seafloor soil. In a previous study, we developed a drilling robot that could excavate 430 mm into the ground while underwater. However, excavation deeper than 430 mm was not possible because the discharging outlet became buried, making it difficult to discharge the drilled soil. In this paper, we develop a discharging mechanism utilizing water jetting to improve the excavation depth to 650 mm and potentially deeper.

INDEX TERMS Drilling robot, underwater excavation, water jetting, seabed exploration, marine robotics.

I. INTRODUCTION

Recently, seabed mineral resources such as rare earth elements have been found on the bottom of the ocean [1], [2]. To utilize these resources, it is necessary to collect and analyze samples [3]. Sampling serves to clarify how seabed mineral resources are generated and distributed. A general sampling method (vertical drilling) is shown on the left side of Fig. 1. In this method, a pipe-shaped sampler is sent from the drillship to the seafloor to collect samples [4]–[6]. There are also seafloor drilling robots such as the Tri-SedimentBot [7], and Human-portable Underwater Robot [8]. By using this method, samples can be obtained continuously without any disturbance. It is useful for acquiring the geological profile in the vertical direction. However, it is inefficient for investigating deposits widely distributed in the horizontal direction because the sampling range is limited to the diameter of the pipe (approximately 100 mm). To solve this problem, this study aims to develop a seafloor robotic explorer that can excavate horizontally and collect samples of rare earth elements. Rare earth elements are deposited 2–3 meters into the deep sea floor [9]. Wide area exploration can be made possible by deploying multiple robots to autonomously search beneath the seabed.

The associate editor coordinating the review of this manuscript and approving it for publication was Yingxiang Liu.

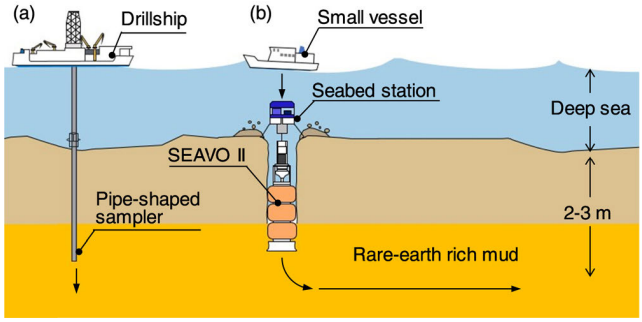

FIGURE 1. (a) General sampling method (vertical drilling). (b) Conceptual representation of SEAVO II (horizontal drilling).

Presently, several drilling robots have been proposed. These drilling robots can be classified into three types: striking penetration type, screw type, and bioinspired. The striking penetration type robots, such as PLUTO [10], MMUM [11], and the Hammer-driven type penetrator [12], penetrate the ground with a striking force. The screw type robots, such as the screw subsurface explorer [13], STSM [14], and the DIGBOT [15], excavate with low torque by rotating a screw. The bioinspired robots include IDDS [16] and IBR [17] that imitate an inchworm, RoboClam [18] which imitates a razor clam, and the actuated bivalve robot [19] that mimics a bivalve. However, these robots are susceptible to

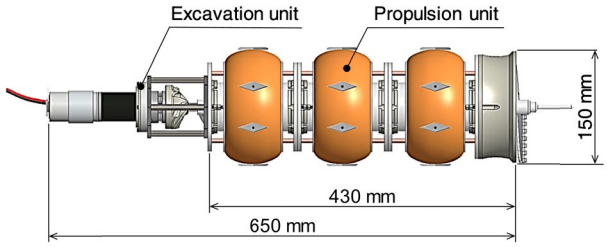

FIGURE 2. Conceptual model of SEAVO II with its excavation and propulsion units. The former is aimed for ground excavation and for creating a space for locomotion, whereas the latter is designed to move by extending and contracting cylinders to imitate the peristaltic motion of an earthworm.

earth pressure, and drilled soils cannot be discharged out of the hole. Therefore, they cannot excavate deep underground.

To overcome these challenges, we focused on the locomotion of an earthworm [20], [21]. Earthworm locomotion is only marginally susceptible to earth pressure [22]. This locomotion method has already been applied to several robots. For example, PEW-RO [23], the origami-inspired worm robot [24], and the mesh-body worm robot [25]. In our previous study, we developed a drilling robot named SEAVO that succeeded in excavating 613 mm at a turning radius of 1670 mm on land [26]. We also developed an underwater drilling robot named SEAVO II which successfully drilled 430 mm into the ground while underwater [27], [28]. Furthermore, we studied drilling methods to reduce the drilling resistance [29], [30]. However, SEAVO II could not excavate deeper than 430 mm because the discharging outlet of SEAVO II became buried in the ground, making it difficult to discharge the drilled soil. Therefore, this paper proposes a discharging mechanism that implements water jetting to improve the excavation depth.

The future operation of SEAVO II is shown on the right side of Fig. 1. The operation is divided into the following five phases: (i) the seabed station carrying SEAVO is dropped from a vessel. (ii) SEAVO II excavates vertically from the seabed station to the target depth (2–3 m). (iii) SEAVO II bends at the target depth, excavates horizontally, and collects samples inside its body. (iv) SEAVO II returns to the seabed station. (v) The seabed station with SEAVO II drops weights and floats up. In this paper, we focus on phase (ii) and discuss a method to achieve the target depth.

The paper is organized as follows. Section II describes the concept of SEAVO II. The concept and model of the discharging mechanism are explained in Section III. Section IV clarifies the properties of the discharging mechanism. In section V, the results of the excavation experiments are discussed. Conclusions and future work are presented in Section VI.

II. DRILLING ROBOT SEAVO II

A. SEAVO II LOCOMOTION

Fig. 2 shows the conceptual model of SEAVO II. SEAVO II consists of two units, an excavation unit and a propulsion unit. The excavation unit excavates the ground and generates a space for locomotion. The propulsion unit moves by

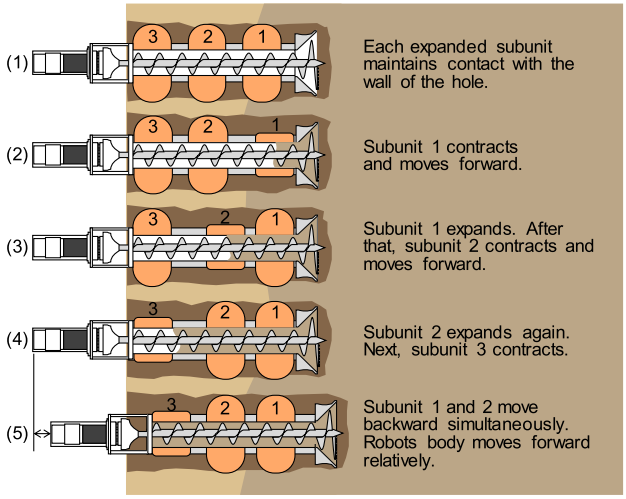

FIGURE 3. Locomotion principle of SEAVO II. A depth of 10 mm is propelled every 75 s by pattern repetition.

extending and contracting cylinders similar to the movement of an earthworm [26]–[30]. Fig. 3 shows the method of SEAVO II locomotion which consists of 5 steps. Each propulsion subunit is named subunit 1, 2, and 3, starting from the top.

(1) Each expanded subunit maintains contact with the wall of the hole.

(2) Subunit 1 contracts and moves forward.

(3) Subunit 1 expands again. After that, subunit 2 contracts and moves forward.

(4) Subunit 2 expands again. Next, subunit 3 contracts.

(5) Subunit 1 and 2 move backward simultaneously. At this point, the robot body moves forward relative to its starting position.

Advantages of this locomotion method include the fact that SEAVO II can move with less susceptibility to earth pressure, and the operation of SEAVO II is not dependent on its weight (gravitational force) because it advances by the propulsive force of cylinders [28].

B. EXCAVATION UNIT

As the excavation unit is principally designed for ground excavation, for discharging of drilled soil from the outlet, and for securing a space for an earthworm-like propulsion, it consists of a motor (RS-775GM504, Suzakugiken), the waterproof case for the motor, a discharging outlet, a casing pipe, an earth auger, and a head part, as systematically illustrated in Fig. 4(a). The earth auger is displayed in Fig. 4(b). The auger head excavates the ground, and the auger screw conveys and discharges the drilled soil [28]. The robot material is made of cut-out aluminum plates and polycarbonate plastic. In addition, some parts were produced with a three-dimensional (3D) printer.

C. PROPULSION UNIT

Fig. 5(a) shows the propulsion unit, and Fig. 5(b) shows its internal structure. It consists of setae [28],

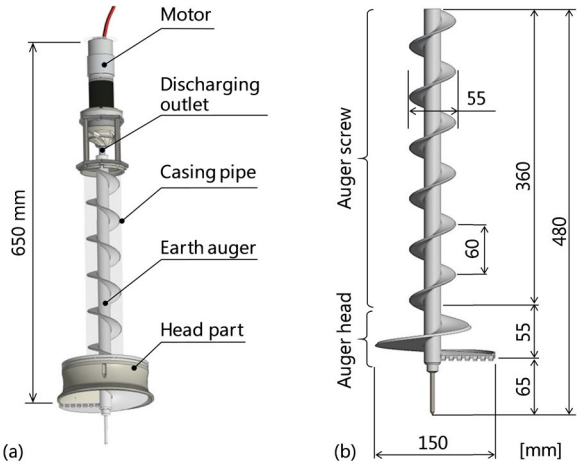

FIGURE 4. (a) Schematic diagram of the excavation unit. (b) Schematic diagram of the earth auger.

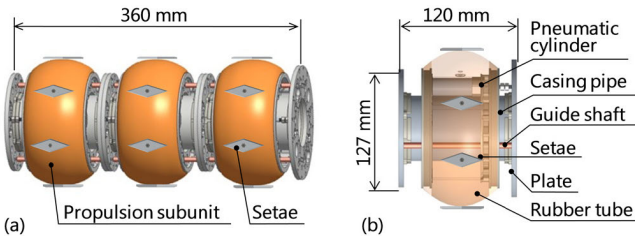

FIGURE 5. (a) A schematic diagram of the propulsion unit in SEAVO II, mainly composed of three propulsion sub-units. (b) Internal structure of the propulsion sub-unit.

plates, a casing pipe, guide shafts, a pneumatic cylinder (CJ2B16-15Z, SMC), and a rubber tube. The setae are part of the mechanism for improving the gripping force. The rubber tube expands with air pressure, and the expansion part slides 10 mm by extending and contracting the cylinder. These propulsion sub-units are connected using bolts and gaskets. Currently, pneumatic actuators are used, but for deep sea applications, hydraulic actuators will be implemented.

III. DISCHARGING MECHANISM UTILIZING WATER JETTING

A. CONCEPT OF THE DISCHARGING MECHANISM USING WATER JETTING

We propose a discharging mechanism based on water jetting. This mechanism is necessary because currently, SEAVO II cannot excavate more than 430 mm while underwater; the discharging outlet gets buried, and it becomes impossible to discharge the drilled soil. For SEAVO II to reach the target depth of 3 m, it is necessary to develop a discharging mechanism that enables SEAVO II to discharge smoothly to remove the drilled soil. One method of discharging involves riserless drilling, during which a hollow drill pipe equipped with a drill bit is rotated by a motor on a drillship to excavate the seafloor ground. As Fig. 6(a) shows, seawater is injected from the tip of the drill bit, and the drilled soil is conveyed and discharged from the hole to the seabed surface [31]. Fig. 6(b) presents the discharging mechanism utilizing water

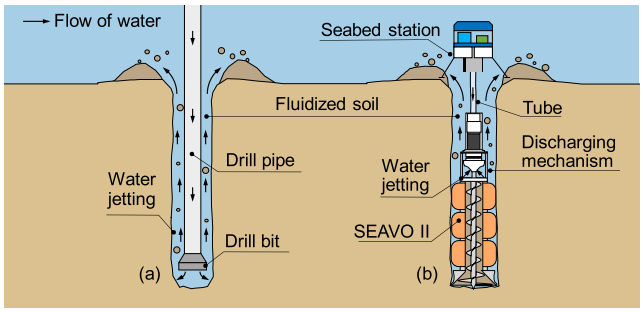

FIGURE 6. (a) Riserless drilling system, and (b) the concept of the discharging mechanism utilizing water jetting.

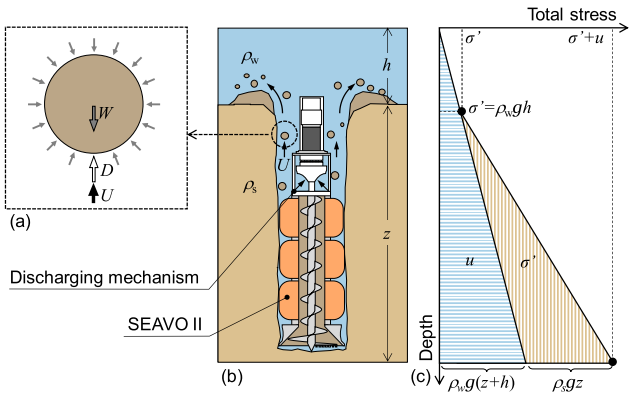

FIGURE 7. (a) Fluidized soil particle, (b) the model of SEAVO II in ground, and (c) stress distribution. Water jetting is effective for fluidization based on Eq. (1), and it is possible to convey and discharge fluidized sand particles to the ground surface based on Eq. (7).

TABLE 1. The parameters of Figure 7.

σ	Total stress	Pa	V	Volume of soil particle	m^3
σ'	Effective stress	Pa	D	Drag force	N
u	Pore water pressure	Pa	W	submerged weight	N
ρ_s	Density of soil	kg/m^3	U	Flow velocity	m/s
ρ_w	Density of water	kg/m^3	A	Cross-sectional area of soil particle	m^2
h	Sea depth	m	C_D	Drag coefficient	
z	Ground depth	m	g	Gravitational acceleration	m/s^2

jetting; in this case, the water intrudes between the sand particles, and the ground becomes fluidized. The fluidized sand is then transferred to the seabed surface by water flow. SEAVO II smoothly discharges the drilled soil and reaches the target depth [32]. The sea water necessary for water jetting is supplied from the seabed station. The motivation for jetting water from the discharging outlet stems from the creation of a cavity that is generated not only in the front but also in the side of SEAVO II when water is injected from the tip of SEAVO II similarly to the riserless drilling. Ultimately, SEAVO II slips and fails to excavate and propel.

B. MODELING OF THE DISCHARGING MECHANISM

Fig. 7 shows the model of SEAVO II buried in the ground, and Table 1 lists the parameters of Fig. 7. To smoothly discharge the drilled soil, it is necessary to (i) fluidize the ground around the discharging outlet by water jetting and (ii) convey the

fluidized sand particles to the seafloor surface by water flow. First, we consider the effectiveness of water jetting on the fluidization. The total stress σ in the underwater ground is given by Eq. (1) [33], [34]:

$$\sigma = \sigma' + u, \tag{1}$$

where σ' is the effective stress, and u is the pore water pressure, given by Eq. (2) and Eq. (3), respectively:

$$\sigma' = \rho_s g z \tag{2}$$

$$u = \rho_w g (h + z). \tag{3}$$

Here, ρ_s is the density of sand, ρ_w is the density of water, g is the gravitational acceleration, z is the ground depth, and h is the sea depth. The effective stress is the only effective factor for ground deformation [35], [36]. If effective stress is reduced, the ground will be fluidized. In this model, the total stress does not change before and after water jetting because the system is completely immersed in sea water, the water level does not change. It is possible to reduce the relative effective stress by increasing the pore water pressure since the total stress does not change. During water jetting, water intrudes between the soil particles, and the pore water pressure increases, thus the ground becomes fluidized by water jetting.

Next, we consider the condition of the flow velocity that enables the fluidized sand particles to be conveyed to the ground surface by water flow. The free body diagram of the sand particles is shown in Fig. 7 (a). The sand particles are subjected to drag force by the upward flow of the jetted water. If the drag force is greater than the submerged weight, i.e., gravitational force minus the buoyancy of the sand particle, the sand particles will be conveyed to the ground surface. This condition is given by Eq. (4),

$$D > W, \tag{4}$$

where W is the submerged weight, and D is the upward drag force. Forces other than the submerged weight, the drag force, and the water pressure are ignored for simplicity. There is no effect due to water pressure because the water pressure acts on the sand particles isotropically. The submerged weight W is given by Eq. (5).

$$W = (\rho_s - \rho_w) Vg, \tag{5}$$

where V is the volume of the soil particle. The drag force D is given by Eq. (6) [37],

$$D = \frac{1}{2}\rho_w U^2 A C_D, \tag{6}$$

where U is the flow velocity of water, A is the cross-sectional area of the soil particles perpendicular to the direction of the water flow, and C_D is the drag coefficient. When solving for U using Eq. (4), Eq. (5), and Eq. (6), Eq. (7) is obtained. Eq. (7) is the condition of the flow velocity that can convey the fluidized sand particles to the ground surface by water flow.

$$U > \sqrt{\frac{2(\rho_s - \rho_w) Vg}{\rho_w A C_D}} \tag{7}$$

Finally, the excess pore water pressure ratio is used as an evaluation index of the fluidization. It is impossible to compare fluidization conditions at different depths by using the pore water pressure because the pore water pressure depends on the depth. Therefore, it is evaluated by using the excess pore water pressure ratio $\Delta u/\sigma'$ which is the ratio between the excess pore water pressure Δu and the effective stress σ'. $\Delta u/\sigma'$ is given by Eq. (8),

$$\frac{\Delta u}{\sigma'} = \frac{u - u_0}{\sigma - u} \tag{8}$$

where u is the pore water pressure after fluidization, u_0 is the pore water pressure before fluidization, and σ is the total stress. $\Delta u/\sigma'$ is an evaluation index commonly used for the evaluation of the liquefaction phenomenon in civil engineering [38].

In summary, water jetting is effective for fluidization based on Eq. (1), and it is possible to convey and discharge fluidized sand particles to the ground surface (Eq. (7)). However, this model does not consider complex soil behavior, the drilling torque, the jetting direction, and the depth. Therefore, in Section IV, we carry out four experiments (flow rate, drilling torque, direction, and depth property). The validity of the model is discussed by comparing the results of the experiments.

IV. PROPERTIES OF THE DISCHARGING MECHANISM

We carry out four experiments to clarify certain properties of the discharging mechanism. Specifically, we study the (A) flow rate, (B) drilling torque, (C) jetting direction, and (D) depth-related properties. In addition, we confirm the validity of the model is described in Section III.

A. FLOW RATE PROPERTIES

Here, we clarify that water jetting is effective for fluidization of the ground. If the water level is constant, the pore water pressure increases, and the effective stress decreases relatively by water jetting. We experimentally verify Eq. (1) and Eq. (7).

1) THEORETICAL VALUE

We find the minimum flow rate at which the fluidized sand particles are conveyed to the ground surface by water flow. First, we substitute the values of the parameters from this experiment into Eq. (7) to obtain the theoretical value of flow velocity U. The values of each parameter are as follows: $\rho_s = 2630$ kg/m^3, $\rho_w = 998$ kg/m^3, $d = 0.21 \times 10^{-3}$ m, $V = \pi d^3/6 = 4.8 \times 10^{-12}$ m^3, $A = \pi d^2/4 = 3.5 \times 10^{-8}$ m^2, $g = 9.8$ m/s^2, and $C_D = 1.0$. We assume the sand is spherical, and the volume V and the representative area A of the sand particle are calculated from the average

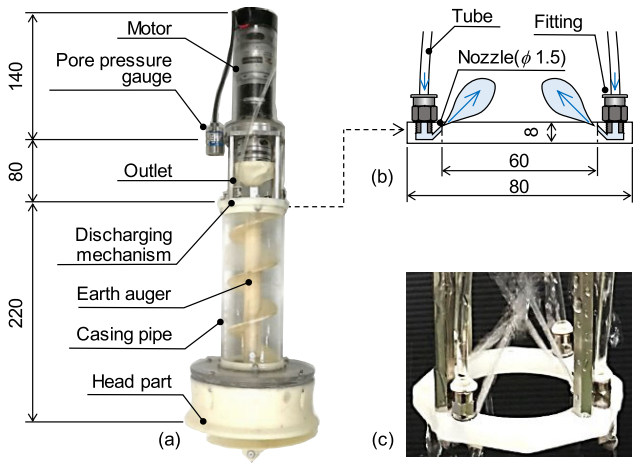

FIGURE 8. (a) Excavation unit with a pore pressure gauge, (b) cross-sectional view of the outlet, and (c) photograph of the water jetting outlet produced with a three-dimensional (3D) printer. The mechanism has four nozzles, each having a diameter of 1.5 mm. The nozzles are positioned symmetrically and diagonally from each other on the discharging mechanism.

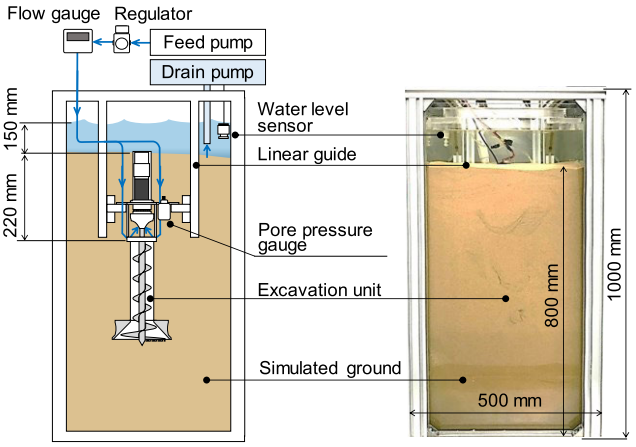

FIGURE 9. Experimental setup with the excavation unit. The pore water pressure gauge is attached to the discharging mechanism.

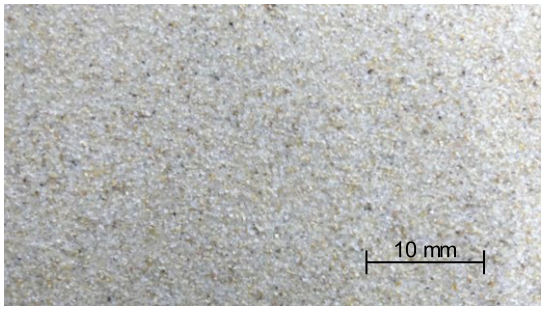

FIGURE 10. The appearance of Toyoura sand.

particle size d. The drag coefficient C_D is set to 1.0 because the flow between the soil particles near the nozzle is generally turbulent. By substituting these parameters into Eq. (7), $U = 66.3 \times 10^{-3}$ m/s obtained. Next, we calculate the minimum flow rate Q from the flow velocity U. The flow rate is given by Eq. (9) since there are four injection nozzles,

$$Q = 4US \tag{9}$$

where S is the cross-sectional area of the nozzle. The values of each parameter are as follows: $U = 66.3 \times 10^{-3}$ m/s, $S = \pi d_{tube}^2/4 = 1.8 \times 10^{-6}$ m^2, and $d_{tube} = 1.5 \times 10^{-3}$ m. Using Eq. (9), the flow rate is calculated to be $Q = 4.7 \times 10^{-7}$ m^3/s = 0.03 L/min, meaning the fluidized sand particles can be conveyed to the ground surface by water jetting at a flow rate of more than 0.03 L/min.

2) EXPERIMENTAL METHOD

Fig. 8 shows photographs (a and c) and a cross-sectional schematic diagram (b) of the discharging mechanism produced with a three-dimensional (3D) printer. The mechanism has four nozzles, each having a diameter of 1.5 mm. The nozzles are positioned symmetrically and diagonally from each other on the discharging mechanism. Fig. 9 shows the experimental setup, consisting of simulated ground, an excavation unit equipped with the discharging mechanism, a pore water pressure gauge (BPR-A-200 KPS, KYOWA), a feed pump, a regulator, a digital flow gauge (6710M-2, KRONE), a water level sensor, and a drain pump. The excavation unit is fixed in its position since the depth from the ground surface to the pore pressure gauge is set to 220 mm. The pore water pressure gauge is attached to the discharging mechanism, as shown in Fig. 8 (a). The flow rate is adjusted from 0 L/min to 1 L/min in 0.1 L/min steps using a digital flow gauge and a regulator. The earth auger is rotated at 20 rpm [28].

The total stress is constant because the water level in the tank was adjusted to constant (150 mm) using the water level sensor and the drain pump. The total stress is calculated as $\sigma = \sigma' + U = \rho_S gz + \rho_w g(h+z) = 9.3$ kPa. Therefore, the effective stress can be calculated from Eq. (1) by measuring the pore water pressure.

3) SIMULATED GROUND

The simulated ground simulates the surface layer of the seafloor. In the actual seafloor, sand, mud, and plankton carcasses etc., are present. Reproducing the actual seafloor is difficult because of the diversity and unevenness of marine sediment. Therefore, Toyoura Sand (Toyoura keiseki kogyo) with a uniform particle size was used as the simulated deposit. The appearance of Toyoura sand is shown in Fig. 10. Table 2 lists the specifications of Toyoura Sand. It is believed that sediment deposits uniformly because deep tide current is very slow, approximately 3.6 m/h. Therefore, the simulated ground is produced by the following procedure. First, we fill the tank with a certain amount of tap water. Next, sand is scattered in small amounts from the top and deposited to a height of 800 mm in the tank, which is 500 mm long, 500 mm wide, and 1000 mm high. In the water saturated sediment, the volume of contained moisture corresponds to the pore volume of the deposit. Therefore, its porosity can be

TABLE 2. Specifications of Toyoura silica sand.

Particle size range and percentage	• Standard copper 300 micron sieve remainder less than 1 %. • Standard copper 106 micron sieve remainder more than 98 %.
Mean particle size	0.21 mm
Soil particle density	2.63 g/cm^3
Presence of organic impurities	No organic impurities found Natural silica sand: 90 %+ silica content
Chemical composition (approx.)	SiO_2 92.6 % Al_2O_3 3.7 % Fe_2O_3 0.7 % CaO 0.5 % MgO 0.2 %

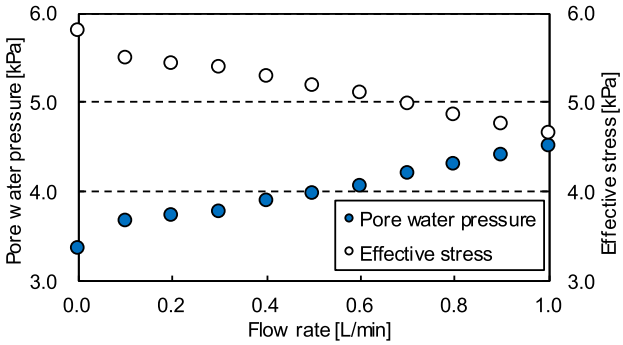

FIGURE 11. Pore water pressure (measured) and effective stress (calculated) versus flow rate. The pore water pressure increases with increasing flow rate, and the effective stress decreases relatively.

calculated from the pore volume, which is 40 %. Considering the influence of water pressure on the seafloor soil, we believe that the water pressure has no influence on the seafloor soil because it acts isotropically on the sand particles. Based on Eq. (1), Eq. (2), and Eq. (3), it is clear that even if the water depth is shallow or deep, the effective stress acting on the sand particles does not change. Thus, the water pressure will have no influence on the seafloor soil.

4) RESULTS AND DISCUSSION

In Fig. 11, the pore water pressure and effective stress values are plotted as dependent on the floor rate. The pore water pressure is a measured value, and the effective stress is a calculated value by using Eq. (1). The pore water pressure increases with increasing flow rate, and the effective stress decreases relatively. The pore water pressure is 3.4 kPa at 0.0 L/min and 3.7 kPa at 0.05 L/min. We assume that the ground became fluidized by water jetting at flow rates above 0.03 L/min. This demonstrates that Eq. (1) and Eq. (7) are reasonable, and that water jetting is effective for fluidization of the ground. Furthermore, this flow rate (0.03 L/min) is very small compared to the flow rate (approximately 50 L/min) in the riser drilling system.

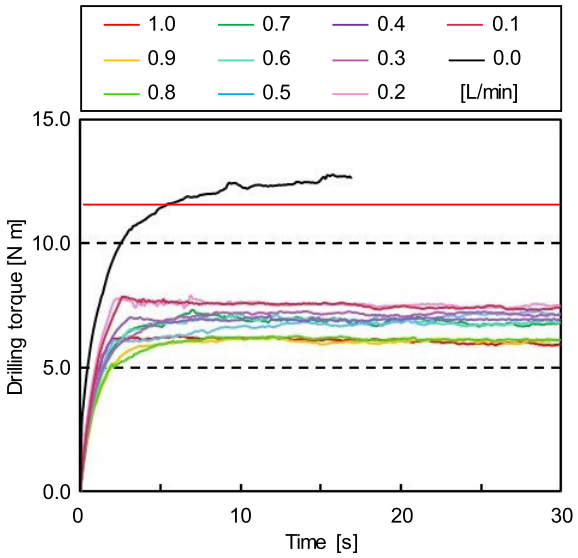

FIGURE 12. Drilling torque with (from flow rate 0.1 to 1.0 L/min) and without (0.0 L/min) water jetting over time. When no water jetting is used, the drilling torque increases dramatically, and it fails to excavate after 17 s. On the other hand, when water jetting is implemented, the drilling torque is lower than the allowable limit, and discharging of the drilled soil is enabled.

B. DRILLING TORQUE PROPERTIES

To determine the target value of the fluidization for adjusting the flow rate, we find the excess pore water pressure ratio when the drilling torque is lower than the allowable limit and when the flow rate is as small as possible. In a previous study, if the drilling torque occurs is higher than 11.6 N m, SEAVO II falls into a "propulsion impossible" mode [25]. Therefore, the allowable limit of the torque is set to 11.6 N m. The experimental method is the same as that in Section IV-A.2. We measure the drilling torque and the pore water pressure, and the experiment starts with the excavation unit being filled with drilled soil. In other words, discharging of the drilled soil begins immediately after the experimental start.

Fig. 12 shows the results of the drilling torque. When no water jetting is used (0.0 L/min flow rate), the drilling torque increases dramatically, and it fails to excavate after 17 s. Discharging the drilled soil is impossible because the discharging outlet is already buried in the ground. The maximum drilling torque is 12.8 N m at 15 s, exceeding the allowable limit. On the other hand, when water jetting is implemented, the drilling torque is lower than the allowable limit, and discharging of the drilled soil is enabled. Fig. 13 shows the average drilling torque and the excess pore water pressure ratio vs flow rate. The average value of the drilling torque is calculated from 10 s after the steady state. At a flow rate of 0.1 L/min, the lowest flow rate, the average drilling torque is lower than the allowable limit of the torque. At this point, the excess pore water pressure ratio is 0.07. If the excess pore water pressure ratio around the discharging mechanism is more than 0.07, the drilled soil can be discharged. Therefore, the target of the excess pore water pressure ratio is set to 0.07.

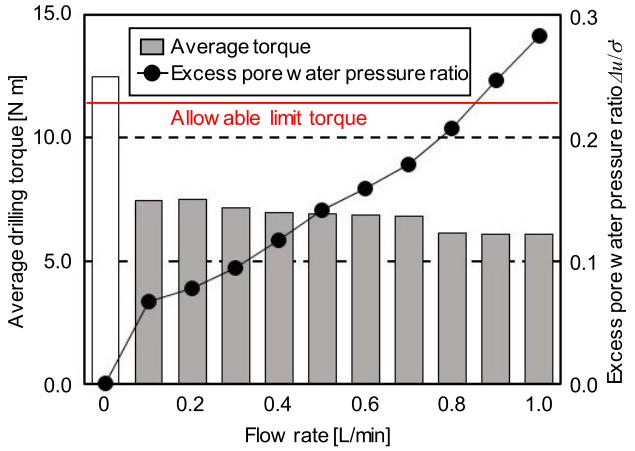

FIGURE 13. Average torque and excess pore water pressure ratio versus the flow rate.

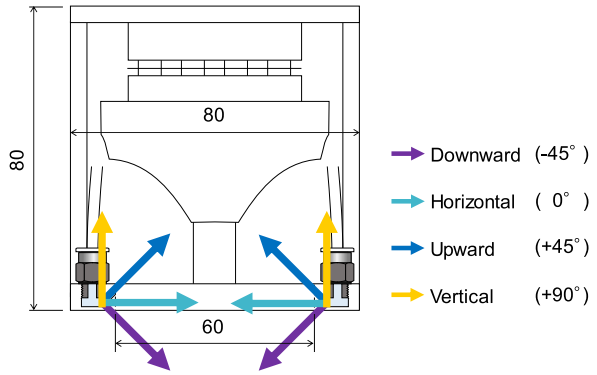

FIGURE 14. Directions of water jetting via the four outlet types.

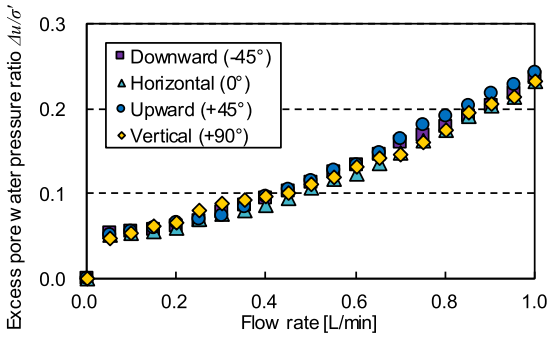

FIGURE 15. Excess pore water pressure ratio versus flow rate based on the direction of the water jetting.

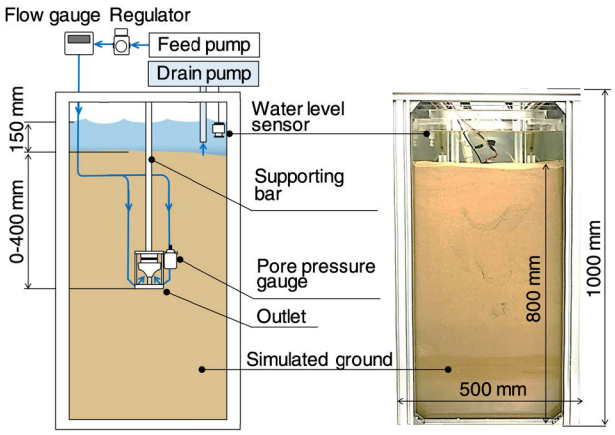

FIGURE 16. Experimental setup for studying the depth properties with the water jetting mechanism.

C. JETTING DIRECTION PROPERTIES

We determine the direction of water jetting that is effective for fluidization by designing four discharging outlets (downward, horizontal, upward, and vertical), as shown in Fig. 14. The downward outlet injects water into the casing pipe at an angle of 45° to fluidize the drilled soil before it passes through the outlet. The horizontal outlet injects water into the outlet horizontally. The upward outlet injects water into the outlet at an angle of 45° to fluidize the drilled soil for smooth discharging. The vertical outlet injects water from the outlet vertically to prevent the inflow of sand from the surroundings. The experimental method is the same as that described in Section IV-A.2. The flow rate is changed from 0 L/min to 1 L/min in 0.05 L/min increments.

Fig. 15 shows the excess pore water pressure ratio versus the flow rate for the different directions of the water jetting. There is no significant difference in the excess pore water pressure ratio for different jetting directions. Therefore, the jetting direction has no influence on fluidization.

D. DEPTH PROPERTIES

Since there is concern regarding the difficulty to fluidize at increased depths, we study how the depth would affect the fluidization. To confirm the usefulness of the discharging mechanism several meters underground, we examine whether the excess pore water pressure ratio at each depth exceeds the target value 0.07. Fig. 16 shows the experimental setup consisting of simulated ground, a discharging mechanism, a pore water pressure gauge (BPR-A-200 KPS, KYOWA), a supporting bar, a feed pump, a regulator, a digital flow gauge (BEVEL BOX BB-180, Niigata Seiki), a water level sensor, and a drain pump. The pore water pressure gauge is attached to the discharging mechanism, as shown in Fig. 16. The flow rate is adjusted using a digital flow gauge and a regulator from 0 to 1 L/min in 0.05 L/min increments. The distance between the ground surface and the discharging mechanism is adjusted by changing the length of the supporting bar. The total stress is constant because the water level in the tank is adjusted to be constant (150 mm deep) by using the water level sensor and the drain pump.

In Fig.17, the excess pore water pressure ratio is shown to decrease with increasing excavation depth. The flow rate when exceeding the target ratio of 0.07 at each depth is more than 0.50 L/min. The influence of water jetting pressure decreases relatively because the pore water pressure before water jetting increases as the depth rises. Therefore, it is necessary to adjust the flow rate so as not to be lower than the excess pore water pressure ratio target value of 0.07.

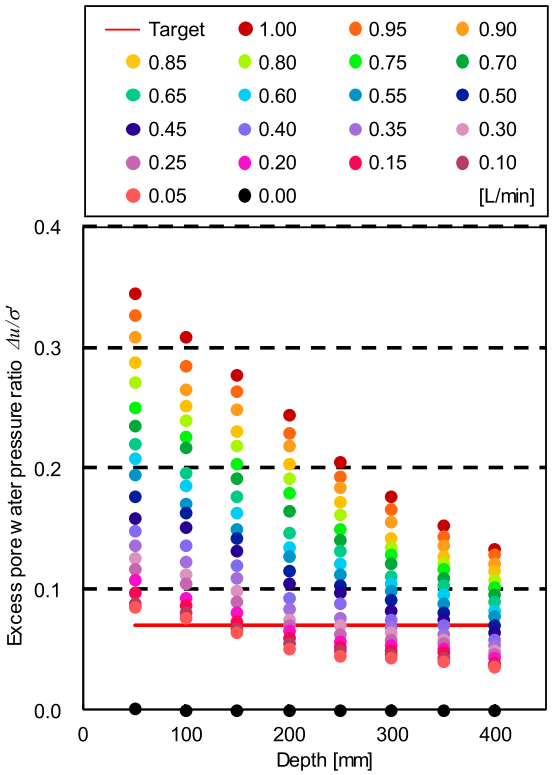

FIGURE 17. Dependence of the excess pore water pressure ratio on the excavation depth and based on the flow rate. The horizontal red line denotes the target ratio of 0.7. The colored dots show the flow rate from 0 (lowest dots) to 1 L/min (top, dark red dots) in increments of 0.05 L/min.

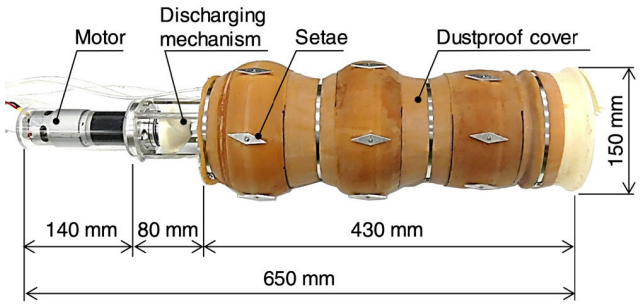

FIGURE 18. Annotated photograph of SEAVO II. SEAVO II is covered with a rubber tube for dustproofing.

V. DRILLING EXPERIMENTS BY SEAVO II

We confirm the usefulness of the discharging mechanism utilizing water jetting by drilling experiments and compare the excavation torque and depth with and without water jetting.

A. EXPERIMENTS METHOD OF SEAVO II

Fig. 18 shows an annotated photograph of SEAVO II. SEAVO II is covered with a rubber tube for dustproofing. Fig. 19 shows the experimental setup. This consists of SEAVO II, a launcher, simulated ground, a wire encoder (D-1000Z-V, MUTOH), a feed pump, a regulator, a digital flow gauge (BPR-A-200 KPS, KYOWA), a water level sensor, and a drain pump. The launcher is the supporting

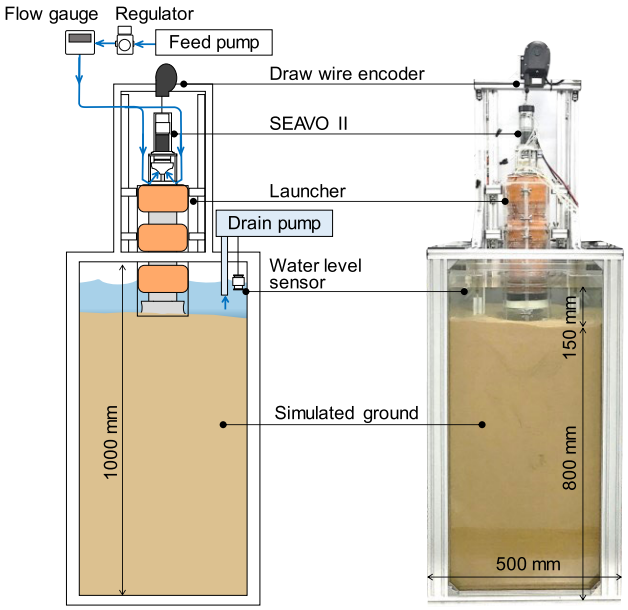

FIGURE 19. Experimental setup with SEAVO II.

frame for SEAVO II. The simulated ground has a water depth of 15 mm and a ground depth of 800 mm. The earth auger rotates at 20 rpm, and the penetration speed is adjusted to 2.3 mm/s [25]. The electric current of the motor is measured and used to calculate the drilling torque. In addition, the excavation depth is measured using the wire encoder. The flow rate of the water jetting is set to 0.5 L/min based on the results presented in Section IV-D. The experiment is terminated when SEAVO II reaches 650 mm, which corresponds to the total length of the excavation robot, because of experimental setup limitations.

B. RESULTS AND DISCUSSION OF THE EXPERIMENT WITHOUT WATER JETTING

Fig. 20 shows the drilling torque and excavation depth for the experiment with no water jetting. After 390 s, SEAVO II begins to discharge the drilled soil from the discharging outlet. The drilled soil deposits around the penetration area. SEAVO II stably excavates up to 450 mm. However, the drilling torque sharply increases after 450 mm. Ultimately, when SEAVO II reaches 568 mm excavation depth at 6748 s, it fails to excavate further. The distance from the tip of the robot to the discharging outlet is 430 mm. After 450 mm, SEAVO II cannot discharge the drilled soil because the discharging outlet is buried.

C. RESULTS AND DISCUSSION OF THE EXPERIMENT WITH WATER JETTING

When water jetting is utilized, SEAVO II excavates 650 mm within 6300 s. In this experiment, the excavation is stopped when SEAVO II reaches 650 mm due to limitations in the experimental setup, as shown in the time-lapse photograph in Fig. 21. Fig. 22 shows the drilling torque and excavation depth. There is no appreciable increase in torque with

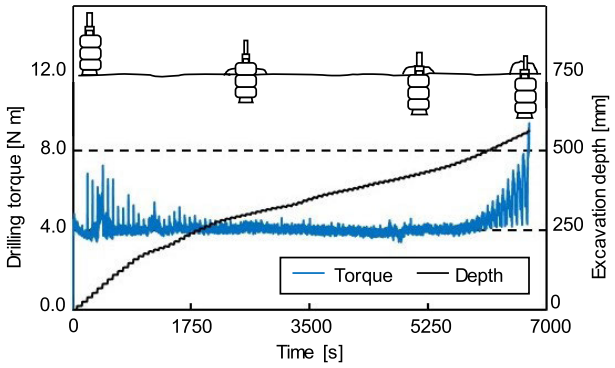

FIGURE 20. Torque and excavation depth over time without implementing water jetting. SEAVO II fell into a "propulsion impossible" mode.

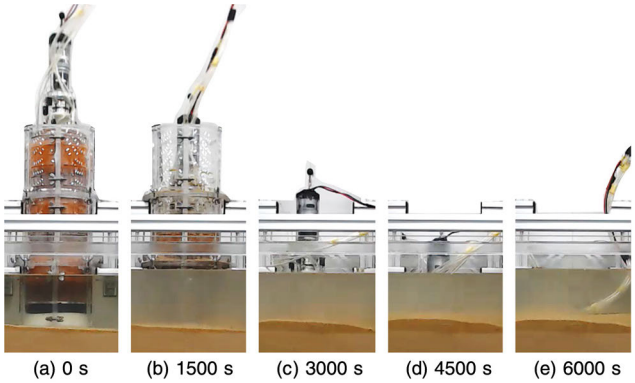

FIGURE 21. The time-lapse photographs of excavation by SEAVO II utilizing water jetting.

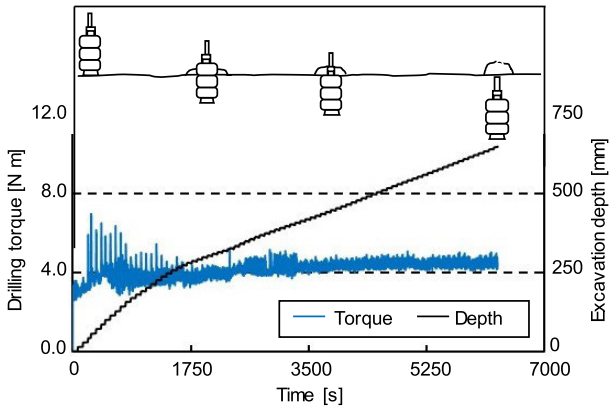

FIGURE 22. Torque and excavation depth over time when water jetting is implemented. SEAVO II succeeded in drilling 650 mm into the ground while underwater.

increasing depth, and in comparison with the experiment without water jetting, there is no change at or deeper than 450 mm. In addition, the excavation depth increases steadily without slowing beyond 450 mm. The discharging mechanism utilizing water jetting generates a fluidized area and transports the drilled soil to the ground surface by water flow, which is clearly visualized during the experiment; the soil appears to blow up from the ground surface. These results confirm the usefulness of the discharging mechanism utilizing water jetting. The experiment is carried out with a flow rate of 0.5 L/min. As a future prospect, we are developing a system that adjusts the flow rate according to the excavation depth, which we believe will enable SEAVO II to reach the target depth of 3 m.

VI. CONCLUSION AND FUTURE WORK

In this paper, we improve the excavation depth and develop a discharging mechanism using water jetting. The obtained results are summarized as follows:

- We propose the discharging mechanism model and experimentally confirm the validity of the model.
- The pore water pressure increases with increasing flow rate, and the effective stress decreases relatively.
- The water jetting direction does not influence the fluidization.
- The pore water pressure decreases with increasing excavation depth.
- SEAVO II with the discharging mechanism succeeds in drilling 650 mm into the ground while underwater. The discharging mechanism enables SEAVO II to smoothly discharge the drilled soil.

In the future, we are developing a control system that adjusts the flow rate according to the excavation depth. In this study, we stopped the experiment when SEAVO II reached 650 mm because the size of the experimental equipment was limited. And, Eq (7) does not hold if the soil contains small gravel. Therefore, we will conduct field experiments to confirm the ability of excavation more than 650 mm. In addition, we plan to develop flexion joints to achieve a directional drilling robot.

REFERENCES

[1] H. Nakajoh, H. Osawa, T. Miyazaki, K. Hirata, T. Sawa, and H. Utsugi, "Development of work class ROV applied for submarine resource exploration in JAMSTEC," in *Proc. OCEANS*, Yeosu, South Korea, May 2012, pp. 1–5, doi: 10.1109/oceans-yeosu.2012.6263437.

[2] S. D. Scott, "Marine minerals: Their occurrences, exploration and exploitation," in *Proc. MTS/IEEE OCEANS KONA*, Sep. 2011, pp. 1–8, doi: 10.23919/oceans.2011.6107119.

[3] X. Zhang, Z. Luan, J. Yan, and C. Chen, "Development of a deep-sea sediment long coring system based on a Jackhammer for R/V Kexue," in *Proc. OCEANS*, Oct. 2012, pp. 1–6.

[4] K. Wada, "Coring technology to be applied in IODP NanTroSEIZE," in *Proc. OCEANS-MTS/IEEE Kobe Techno-Ocean*, Apr. 2008, pp. 1–4, doi: 10.1109/oceanskobe.2008.4531001.

[5] M. Kyo, "Challenges to drill through seismogenic zone," in *Proc. IEEE Int. Underwater Technol. Symp. (UT)*, Mar. 2013, pp. 1–7, doi: 10.1109/UT.2013.6519908.

[6] T. Mcginnis, "Remote control seafloor coring in the west Mariana basin," in *Proc. OCEANS MTS/IEEE. Riding Crest 21st Century Conf. Exhib.*, Jan. 2003, pp. 255–256.

[7] J. Han Bae, J. Hwan Park, S. Lee, and B.-C. Min, "Tri-SedimentBot: An underwater sediment sampling robot," in *Proc. IEEE Int. Conf. Autom. Sci. Eng. (CASE)*, Aug. 2016, pp. 1360–1365.

[8] N. Sakagami, S. Sasaki, M. Kawabata, K. Yokoi, S. Matsuda, A. Mitsui, K. Sano, K. Tago, and S. Kawamura, "Development of a human-portable underwater robot for soil core sampling," in *Proc. MTS/IEEE OCEANS*, Bergen, Norway, Jun. 2013, pp. ,–130128.

[9] Y. Kato, K. Fujinaga, K. Nakamura, Y. Takaya, K. Kitamura, J. Ohta, R. Toda, T. Nakashima, and H. Iwamori, "Deep-sea mud in the Pacific Ocean as a potential resource for rare-earth elements," *Nature Geosci.*, vol. 4, no. 8, pp. 535–539, Aug. 2011.

[10] L. Richter, P. Coste, V. V. Gromov, and A. Grzesik, "The mole with sampling mechanism(MSM)-technology development and payload of beagle 2 mars lander," in *Proc. 8th ESA Workshop Adv. Space Technol. Robot. Autom.*, 2007, pp. 2–4.

[11] C. R. Stoker, A. Gonzales, and J. R. Zavaleta, "Moon/mars underground mole," in *Proc. NASA Sci. Technol. Conf.*, 2008, pp. 1–7.

[12] Y. Shen, S. Jiang, C. Xu, W. Zhang, and X. Wu, "Study on optimization of structure parameters to the penetrator," in *Proc. IEEE Int. Conf. Mechatronics Autom.*, Aug. 2016, pp. 1518–1523.

[13] K. Nagaoka, T. Kubota, M. Otsuki, and S. Tanaka, "Robotic screw explorer for lunar subsurface investigation: Dynamics modelling and experimental validation," in *Proc. IEEE Int. Conf. Robot. Automat.*, Jun. 2009, pp. 1–6.

[14] S. Yasuda, K. Komatsu, and S. Tanaka, "Self-turning screw mechanism for burying geophysical sensors under regolith," in *Proc. Int. Symp. Artif. Intell., Robot. Automat. Space*, 2012, p. 09B02.

[15] R. Abe, Y. Kawamura, K. Kamijima, K, Murakami, "Performance evaluation of contra-rotating drill for DIGBOT," in *Proc. SICE Annu. Conf.*, 2010, pp. 885–888.

[16] S. P. Gorevan, K. Y. Kong, T. M. Myrick, P. W. Bartlett, S. Singh, S. Stroescu, Roopnarine, and S. Rafeek, "An inchworm deep drilling system for kilometer scale subsurface exploration of mars (IDDS) forum on innovative approaches to outer planetary," in *Proc. Concepts Approaches Mars Explor.*, 2004, pp. 1394–1399.

[17] W. Zhang, S. Jiang, Y. Shen, P. Li, and H. Chen, "Development of an inchworm-type drilling test-bed for planetary subsurface exploration and preliminary experiments," in *Proc. IEEE Int. Conf. Robot. Biomimetics (ROBIO)*, Dec. 2016, pp. 2187–2191.

[18] A. G. Winter, R. L. H. Deits, D. S. Dorsch, A. E. Hosoi, and A. H. Slocum, "Teaching RoboClam to dig: The design, testing, and genetic algorithm optimization of a biomimetic robot," in *Proc. IEEE/RSJ Int. Conf. Intell. Robots Syst.*, Oct. 2010, pp. 4231–4235.

[19] A. Koller-Hodac, D. P. Germann, A. Gilgen, K. Dietrich, M. Hadorn, W. Schatz, and P. Eggenberger Hotz, "Actuated bivalve robot study of the burrowing locomotion in sediment," in *Proc. IEEE Int. Conf. Robot. Autom.*, May 2010, pp. 1209–1214.

[20] H. Omori, T. Hayakawa, and T. Nakamura, "Locomotion and turning patterns of a peristaltic crawling earthworm robot composed of flexible units," in *Proc. IEEE/RSJ Int. Conf. Intell. Robots Syst.*, Sep. 2008, pp. 1630–1635.

[21] H. Omori, T. Murakami, H. Nagai, T. Nakamura, and T. Kubota, "Planetary subsurface explorer robot with propulsion units for peristaltic crawling," in *Proc. IEEE Int. Conf. Robot. Autom.*, May 2011, pp. 649–654.

[22] R. M. Alexander, *Exploring Biomechanics Animals in Motion*. San Francisco, CA, USA: Freeman, 1992, pp. 77–79.

[23] Y. Mano, R. Ishikawa, Y. Yamada, and T. Nakamura, "Development of contraction force control system of peristaltic crawling robot for sewer pipe inspection," in *Proc. IEEE/ASME Int. Conf. Adv. Intell. Mechatronics (AIM)*, Jul. 2018, pp. 936–941.

[24] C. D. Onal, R. J. Wood, and D. Rus, "An origami-inspired approach to worm robots," *IEEE/ASME Trans. Mechatronics*, vol. 18, no. 2, pp. 430–438, Apr. 2013.

[25] Y. Huang, A. Kandhari, H. J. Chiel, R. D. Quinn, and K. A. Daltorio, "Slip reduction controls of mesh-body worm robot developed from a mathematical model," in *Proc. IEEE Int. Conf. Robot. Biomimetics (ROBIO)*, Dec. 2017, pp. 1474–1479.

[26] N. Tadami, M. Nagai, T. Nakatake, A. Fujiwara, Y. Yamada, T. Nakamura, H. Yoshida, H. Sawada, and T. Kubota, "Curved excavation by a subseafloor excavation robot," in *Proc. IEEE/RSJ Int. Conf. Intell. Robots Syst. (IROS)*, Sep. 2017, pp. 4950–4955.

[27] N. Tadami, K. Isaka, T. Nakatake, A. Tujiwara, Y. Yamada, T. Nakamura, M. Sugesawa, and H. Yoshida, "Underwater excavation by excavation robot equipped with propulsion unit based on earthworm setae," in *Proc. IEEE Int. Conf. Robot. Biomimetics (ROBIO)*, Dec. 2018, pp. 51–58, doi: 10.1109/robio.2018.8664782.

[28] K. Isaka, K. Tsumura, T. Watanabe, W. Toyama, M. Sugesawa, Y. Yamada, H. Yoshida, and T. Nakamura, "Development of underwater drilling robot based on earthworm locomotion," *IEEE Access*, vol. 7, pp. 103127–103141, 2019.

[29] K. Isaka, N. Tadami, A. Fujiwara, T. Nakatake, M. Suzesawa, Y. Yamada, H. Yoshida, and T. Nakamura, "Water jetting excavation and consideration of earth auger shape to reduce drilling torque for seabed robotic explorer," in *Proc. IEEE/ASME Int. Conf. Adv. Intell. Mechatronics (AIM)*, Jul. 2018, pp. 887–892.

[30] K. Isaka, N. Tadami, A. Fujiwara, T. Watanabe, M. Sugesawa, Y. Yamada, H. Yoshida, and T. Nakamura, "Study on drilling resistance reduction of a seafloor robotic explorer based on the drilling properties of underwater ground," in *Proc. IEEE/SICE Int. Symp. Syst. Integr. (SII)*, Jan. 2019, pp. 718–723, doi: 10.1109/sii.2019.8700347.

[31] K. Wada, M. Saito, and H. Yamaguchi, "Development of the waste mud treatment system for drilling vessel 'CHIKYU,"' in *Proc. OCEANS-Asia Pacific*, May 2006, pp. 1–8, doi: 10.1109/oceansap.2006.4393841.

[32] K. Isaka, N. Tadami, A. Fujiwara, T. Watanabe, M. Okui, T. Nakamura, M. Sugesawa, and H. Yoshida, "Soil discharging mechanism for seafloor drilling robot," in *Proc. Int. Conf. climbing Walking Robots Support Technol. Mobile Mach.*, 2019, pp. 219–225.

[33] C. Zet, C. Fosalau, and D. Petrisor, "Pore water pressure sensor for landslide prediction," in *Proc. IEEE SENSORS*, Nov. 2015, pp. 1–4, doi: 10.1109/icsens.2015.7370264.

[34] A. M. D. C. Bandara, L. I. N. De Silva, and Y. W. R. Amarasinghe, "Development of an earth pressure cell to evaluate the total and effective stresses of soil," in *Proc. Moratuwa Eng. Res. Conf. (MERCon)*, May 2018, pp. 527–532, doi: 10.1109/mercon.2018.8421980.

[35] K. Terzaghi, "The shearing resistance of saturated soils," in *Proc. 1st Inc. Conf. Soil Mech.*, vol. 1, 1963, pp. 54–56.

[36] A. W. Skempton, *Terzaghi's Discovery of Effective Stress From Theory to Practice in Soil Mechanics-Selection From the Writings of Karl Terzaghi*. Hoboken, NJ, USA: Wiley, 1996, pp. 42–55.

[37] H. Pazwash and J. M. Robertson, "Forces on bodies in Bingham fluids," *J. Hydraulic Res.*, vol. 13, no. 1, pp. 35–55, Jan. 1975.

[38] J. Wu, A. Kammerer, M. Riemer, R. Seed, and J. Pestana, "Laboratory study of liquefaction triggering criteria," in *Proc. 13th World Conf. Earthq. Eng.*, 2004, Paper 2580.

KEITA ISAKA received the B.S. degree from the Department of Precision Mechanics, Chuo University, Tokyo, Japan, in 2018, where he is currently pursuing the master's degree. His research interest includes the research and development of a seafloor robotic explorer based on earthworm locomotion.

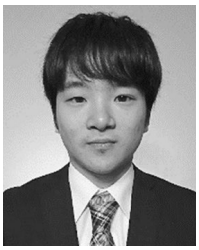

KAZUKI TSUMURA received the B.S. degree from the Department of Precision Mechanics, Chuo University, Tokyo, Japan, in 2019, where he is currently pursuing the master's degree. His research interest includes the research and development of a seafloor robotic explorer based on earthworm locomotion.

TOMOKI WATANABE received the B.S. degree from the Department of Precision Mechanics, Chuo University, Tokyo, Japan, in 2019, where he is currently pursuing the master's degree.

His research interest includes the research and development of a lunar surface explorer based on earthworm locomotion.

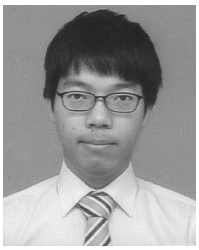

WATARU TOYAMA is currently pursuing the master's degree with Chuo University. His research interest includes the research and development of a lunar surface explorer based on earthworm locomotion.

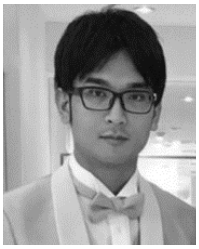

MANABU OKUI received the B.S. and M.S. degrees in mechanical engineering from the Tokyo Institute of Technology, Tokyo, Japan, in 2012 and 2014, respectively. He joined Nissan Motor Company Ltd., in 2014. From 2016 to 2018, he was a Research Assistant with the Research and Develop Initiative, Chuo University, Tokyo. Since 2018, he has been an Assistant Professor with the Research and Develop Initiative.

HIROSHI YOSHIDA graduated from the Tokyo Metropolitan College of Technology, Tokyo, Japan, in 1985. He received the Ph.D. degree from the Graduate School of Natural Science and Technology, Kanazawa University, Kanazawa. Japan, in 1999. In 2002, he joined the Japan Agency for Marine-Earth Science and Technology. His research interests include a seafloor robotic explorer and marine robotic.

TARO NAKAMURA (Member, IEEE) was born in 1975. He received the B.S. and M.S. degrees in mechanical engineering from Akita University, Akita, Japan, in 1997 and 1999 respectively, and the Ph.D. degree from Shinshu University, Nagano, Japan, in 2003. From 1999 to 2003, he taught as a Research Associate with Akita Prefecture University, Akita. In 2004, he taught as a Lecturer with the Faculty of Science and Engineering, Chuo University. From 2006 to 2013, he was an Associate Professor with Chuo University, Tokyo, Japan, where he has been a Professor, since 2013. From 2012 to 2013, he was working as a Visiting Professor with the Swiss Federal Institute of Technology Lausanne, EPFL, Lausanne, Switzerland. He is also working as a CEO at Solaris Inc. His research interests include development and control, such as an artificial muscle, functional fluid, and development and applications of biorobotics.